Applied Catalysis B: Environmental 197 (2016) 86–94

Contents lists available at ScienceDirect

Applied Catalysis B: Environmental

journal homepage: www.elsevier.com/locate/apcatb

# $CeO_2$-modified $Au/TiO_2$ catalysts with outstanding stability under harsh CO oxidation conditions

E. del Río, A.B. Hungría, M. Tinoco, R. Manzorro, M.A. Cauqui, J.J. Calvino, J.A. Pérez-Omil*

*Departamento de Ciencia de los Materiales e Ingeniería Metalúrgica y Química Inorgánica Facultad de Ciencias, Universidad de Cádiz, Campus Río San Pedro, Puerto Real, 11510 Cádiz, Spain*

ARTICLE INFO

*Article history:*
Received 5 January 2016
Received in revised form 15 April 2016
Accepted 16 April 2016
Available online 19 April 2016

Dedicated to Prof. Serafín Bernal for his pioneering work on ceria catalysts at the University of Cádiz.

*Keywords:*
Gold nanoparticles stabilization
Ceria nanolayers
High temperature conditions
CO oxidation
Electron microscopy

ABSTRACT

The 1.5 wt% $Au/TiO_2$ World Gold Council catalyst (WGC) was modified by depositing on its surface a 5.4 wt% $CeO_2$ loading by incipient wetness impregnation. Calcination at 673 K of the resulting, surface-modified, catalyst yielded a material in which the system of gold particles was not significantly modified with respect to that of the starting 1.5% $Au/TiO_2$ WGC catalyst, neither in terms of its size distribution or metallic dispersion. The latter parameter remained, as in the catalyst prior to $CeO_2$ deposition, in a value about 36%. Both catalysts, $Au(1.5\%)/TiO_2$ WGC and $CeO_2(5.4\%)/Au(1.5\%)/TiO_2$, were tested in consecutive CO oxidation reaction loops at increasing final temperatures. In these cycles, the ceria-modified catalyst showed not only a higher activity but, more importantly, a largely enhanced stability against deactivation. Scanning Transmission Electron Microscopy (STEM) studies clearly revealed the presence of nanometer-sized ceria rafts, less than 1 nm thick, on the surface of the fresh $CeO_2(5.4\%)/Au(1.5\%)/TiO_2$ catalysts. After the CO oxidation test at the highest temperature, 1223 K, the WGC catalyst suffered from a very severe Au nanoparticle sintering whereas Au nanoparticle growth was very much limited in the ceria-modified catalyst after the same aging test. STEM results reveal that a major fraction of the Au nanoparticles (75%), comprising all the smaller ones (< 5 nm), was contacting the ceria phase. This evidences an important stabilizing effect of the proposed surface modification. Moreover, these results open up possibilities for gold catalysts in applications where high temperatures are reached under working conditions.



## 1. Introduction

The excellent catalytic performance of gold nanoparticles in energy production related processes such as low temperature CO oxidation [1–4], PROX [5] and WGS [6,7] reactions has been sufficiently demonstrated. All these processes benefit from the unique catalytic properties of gold nanoparticles finely dispersed on metal oxides supports [8–10]. Modified Incipient Wetness Impregnation or Deposition-Precipitation are the methods more widely used for the preparation of these catalysts [2,11,12]. Apart from the particle size, the morphology of gold aggregates is also considered as a key factor for this singular catalytic behavior [3,13,14]. It has been also reported that, in the case of CO oxidation, the amount of chemisorbed molecules is related to the fraction of gold atoms with a reduced coordination number exposed on the surface of the nanoparticles [15]. In this sense, many efforts have been devoted in the last decade to design new synthetic approaches leading to tailored gold catalytic nanostructures [16].

The effect of the support and/or the presence of different kinds of promoters on the catalytic performance of gold have also been investigated, and a general agreement about the advantages of using reducible oxides and, in particular, ceria-based mixed oxides is deduced from a revision of the most recent literature [17,18]. It is thus recognized that the interaction between gold particles and ceria leads to highly dispersed metal systems with improved properties in terms of both activity and stability under reaction conditions. Changes in the electronic and structural properties of the gold particles as a consequence of the metal-support interactions have also been argued to explain the catalytic response of $CeO_2$ and ceria based mixed oxides [4,19–22].

Gold catalysts have also proven to be active in environmental reactions as those occurring in the catalytic converters for depuration of exhaust gases in vehicles. Apart from the well-known capability of gold for the low temperature CO oxidation, some patent also revealed its good activity in the oxidation of hydrocarbons, which favorably compares with that of Pt or Pd, the precious metals currently used in three-way catalysts (TWC) [23]. The use

* Corresponding author.
*E-mail address:* jose.perez-omil@uca.es (J.A. Pérez-Omil).

http://dx.doi.org/10.1016/j.apcatb.2016.04.037
0926-3373/

of gold as a component of the current TWC formulations, substituting the more expensive Pt and Pd, would only be feasible if the excellent catalytic properties of this metal could be maintained after exposure at high temperature operating conditions. In effect, one of the main requirements for a TWC is the ability to oxidize hydrocarbons in a wide temperature range, thus carrying out the catalytic function both in the normal operation of the engine at high temperature (450 °C–1000 °C) and also in the short period at low temperature (<300 °C) following the cold start of the vehicle. However, as it is well known, the major drawback of gold lies in its very poor thermal stability. Due to its melting point (1337 K), relatively low compared with other noble metals (Pd: 1828 K, Pt: 2041 K), gold suffers a severe sintering process starting at temperatures of around 473 K. Sintering involves the transformation of the initial nanoparticles into larger aggregates, thus causing the irreversible deactivation of the catalyst.

Some strategies to prevent the thermal deactivation of gold nanoparticles have been reported so far. Most of them imply special preparation methods or a support modification in order to increase the adherence of gold nanoparticles once they are deposited [24–29]. In all these contributions there is an increase in the complexity of the system or the preparation process. In ref. [29] a high stability is reported for CO oxidation and $CH_4$ combustion at reaction temperatures as high as 600 and 800 °C, respectively. Moreover, it has been reported that the thermal stability of gold nanoparticles could be enhanced just by the deposition through impregnation of amorphous silica on top of a conventional $Au/TiO_2$ catalyst [30]. The catalytic activity of this system, $SiO_2/Au/TiO_2$, is superior to a conventional catalyst where the gold nanoparticles are supported on $SiO_2/TiO_2$, thus pointing out the importance of the addition order during the preparation process. They also indicate the relevance of the singular interactions between the gold nanoparticles and the deposited silica in the performance of this kind of preparations. Hence, this contribution confirms that gold nanoparticles can be stabilized on a current and tested system just by an easy and straight synthetic method.

However, these advances are insufficient and additional improvements must be achieved in order to propose gold catalysts as candidates for high temperatures reactions (>1000 °C) as those occurring in TWC converters.

Taking into account the interactions established between ceria and gold in conventional $Au/CeO_2$ catalysts reported elsewhere [19], it would be interesting to study the effects of depositing ceria on a conventional gold catalyst. With this in mind, the contribution of this paper focuses on an in depth study of the deactivation phenomena in a reference gold catalyst, like $Au/TiO_2$, as well as on comparing the chemical behavior of this system at high temperatures after the addition of a small amount of ceria by a simple incipient wet impregnation method. The major goal of this study is to analyze the change in stability of gold nanoparticles deposited on a commercial catalyst just by a simple single-step post-synthesis modification with small amounts of ceria.

In order to follow the structural evolution of the system at the nanoscale, the samples have been investigated by Scanning Transmission Electron Microscopy both before and after several reaction cycles of CO oxidation at increasing temperatures. Elemental maps recorded using a Cs-corrected Electron Microscope have allowed us imaging the spatial distribution of ceria around the gold nanoparticles. The results reported in this paper show the beneficial effects of the interaction between the gold nanoparticles and the ceria added by impregnation. These results will help to extend the use of gold catalysts in TWC converters as well as in other high temperature technological applications.

On the other hand, the results in this paper will show that the performance of the prepared $CeO_2/Au/TiO_2$ system is comparable to that of $Au/CeZrO_4$ catalyst, i.e. based on bulk forms of ceria. Taking into account that the amount of ceria added to the $Au/TiO_2$ catalyst is very small in comparison to a conventional $Au/CeZrO_4$ catalyst, the preparation of $CeO_2/Au/TiO_2$ systems can be regarded as a feasible method to reduce the amount of lanthanide elements in the formulation of current catalysts, in agreement with recent EU and US DoE recommendations [31–33].

## 2. Experimental

The commercial $Au(1.5\%)/TiO_2$ (World Gold Council) catalyst, with a surface area (BET) of 52 $m^2/g$, was used as a reference sample. The $CeO_2/Au/TiO_2$ system, with a surface area (BET) of 60 $m^2/g$, was prepared by Incipient Wet Impregnation starting from the reference sample and using a 0.35 M $Ce(NO_3)_3{\cdot}6H_2O$ aqueous solution. The pore volumes of the samples were 0.52 $cm^3/g$ and 0.32 $cm^3/g$, respectively. The final ceria loading measured by ICP-AES was 5.4 wt%, this corresponding approx. to half a $CeO_2$ monolayer coverage. A reference ceria-zirconia supported gold catalyst with a 2.6 wt% metal loading was prepared by deposition–precipitation with urea using $H[AuCl_4]$ (Alfa Aesar, 99.99%) as Au precursor [2]. The mixed oxide support used for this reference catalyst, $Ce_{0.62}Zr_{0.38}O_2$ (SBET = 68 $m^2/g$), was kindly donated by Grace Davison.

Prior to characterization or catalytic activity tests, both samples were submitted to an oxidizing activation treatment, under a 60 STP $cm^3\ min^{-1}$ flow of $5\%O_2$/He, at 673 K for 1 h. Then the gas flow was switched, at the same temperature, to pure He and slowly cooled down to room temperature, also under He.

Catalysts were characterized by High Angle Annular Dark Field Scanning Transmission Electron Microscopy (HAADF-STEM) using a JEOL-2010F microscope with a structural resolution of 0.19 nm in TEM. HAADF-STEM images were recorded using a 0.5 nm electron probe at a camera length of 10 cm. The microscope was equipped with an X-ray Energy Dispersive Spectrometer (X-EDS) from Oxford Instruments, model Xmax SSD, for compositional analysis at the subnanometer scale.

Additionally, very high spatial resolution X-EDS maps were acquired using the ChemiSTEM capabilities of a FEI Titan$^3$ Themis 60–300 microscope. In this case, a high brightness, sub-angstrom (0.07 nm) diameter, electron probe was combined with a highly stable stage to record these maps. Maps were acquired with a screen current of 200 pA and a pixel dwell time of 170 μs. This dwell time results in a frame acquisition time of approximately 25 s after which the drift was corrected using cross correlation. An averaging filter was used on the images as provided in the Esprit software.

Samples for STEM studies were prepared by depositing a small amount of the catalyst powders onto holey-carbon coated Cu grids. The use of solvents was avoided during this preparation to minimize carbon contamination effects during the observation in the microscope.

Composition at the macroscopic level was determined by means of ICP-AES in an Iris Intrepid equipment from Thermo. BET surface areas and pore size distribution were obtained via $N_2$ physisorption at 77 K using an Autosorb iQ3 equipment from Quantachrome Instruments. 50–100 mg of the samples were degassed in vacuum at 473 K for 2 h prior to the BET surface analysis. Powder X-ray diffraction experiments were performed using a Bruker B8ADVANCE A25 Davinci equipment.

Catalytic CO oxidation tests were carried out using in all cases 25 mg of the catalyst samples diluted with 100 mg of quartz and placed in a U-shape quartz reactor with a diameter of 7 mm working at atmospheric pressure. The reactant gases stream was a $CO{:}O_2$ mixture in 10:6 molar ratio, balanced with inert gas (He) and flowing with a total spatial velocity of 240000 $cm^3\ h^{-1}\ g^{-1}$. The content (%vol) of the reactant gases were 1% CO, 0.6% $O_2$ and 98.4% He.

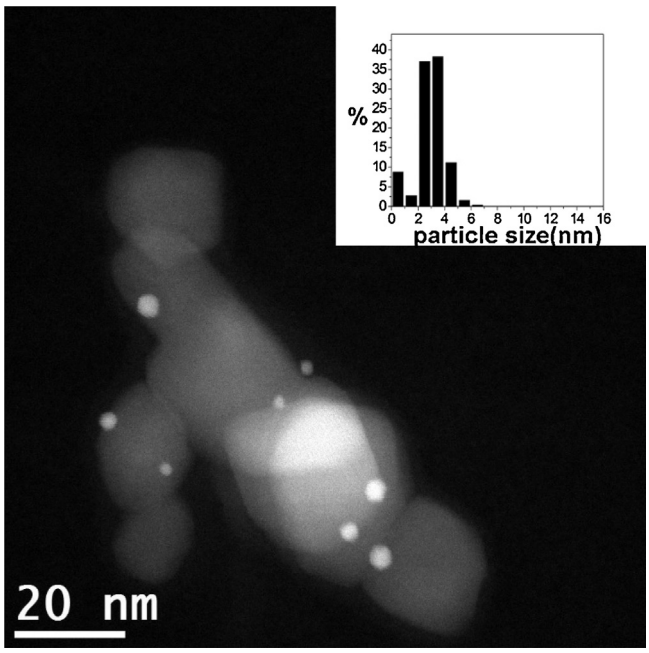


**Fig. 1.** Representative HAADF-STEM image recorded on the starting Au(1.5%)/$TiO_2$ WGC catalyst. The Au particle size distribution is included as inset.

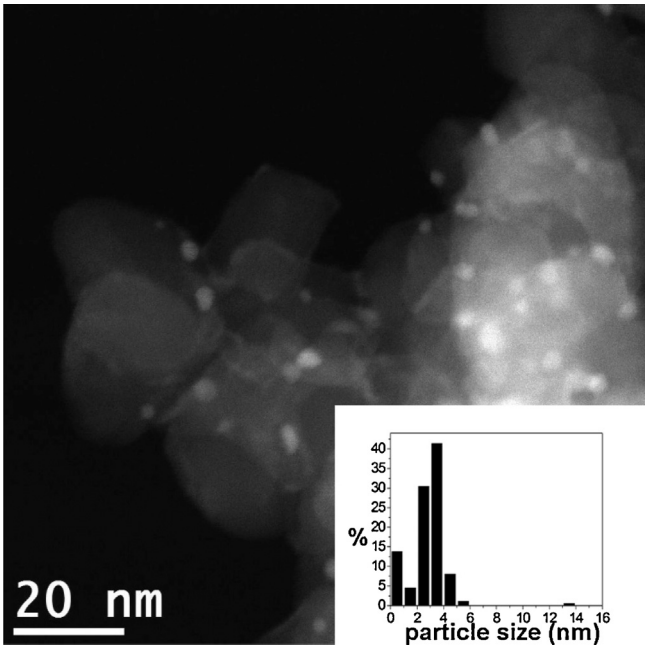


**Fig. 2.** Representative HAADF-STEM image recorded on the as-prepared $CeO_2$(5.4%)/Au(1.5%)/$TiO_2$ catalyst. The Au particle size distribution is included as inset.

The heating rate during the catalytic essays was in all cases of 10 K $min^{-1}$. The gas flow rates were adjusted by mass flow controllers, model Bronkhorst. The gas composition at the reactor exit was continuously monitored by a quadrupole mass spectrometer, Pfeiffer Vacuum Prisma, model QME-200-D.

The catalytic activity was measured in several, consecutive, heating-cooling cycles whose final temperature was increased as follows: 523 K, 623 K, 773 K, 923 K and 1223 K. Linear ramps of 10 K $min^{-1}$ were used during the heating part of the cycles. After reaching each final temperature, the samples were kept under isothermal reaction conditions for 1 h and then freely cooled down, also under the reaction mixture, down to room temperature (RT) before starting the next reaction cycle. To illustrate this, after the initial oxidizing activation treatment, a first CO oxidation test was performed heating from RT up to 523 K. After 1 h under the reaction mixture at 523 K, the sample was cooled down again to RT under the reaction mixture, and then a new cycle was initiated. The final temperature of the heating part of this second cycle was, as previously mentioned, 623 K. After the cycle ending at 1223 K, a final CO oxidation measurement was performed up to a final temperature of 1223 K. This means that 6 different CO oxidation curves were measured for each sample.

## 3. Results and discussion

### 3.1. Characterization of the starting catalysts

The Au(1.5%)/$TiO_2$ WGC catalyst used in this paper is a well characterized commercial sample [34]. The support, $TiO_2$ P25, is made up of a mixture of the anatase and rutile polymorphs in approx. 80/20 molar ratio [35]. This sample was characterized by HAADF-STEM, a technique that allows obtaining images sensitive to the atomic number. Thus, Fig. 1 shows a representative image of the reference catalyst. Note the presence of two different kinds of particles; ones depicting low brightness and size in the range of a few tens of nanometers and a second type of much brighter and much smaller (between 1 and 6 nm) particles. The former corresponds to the $TiO_2$ support ($Z_{Ti}$ = 22) crystallites whereas the latter corresponds to the Au nanoparticles ($Z_{Au}$ = 79). The support oxide particles exhibit irregular morphologies and size between 20 and 80 nm. Powder X-ray Diffraction diagrams show peaks corresponding to both $TiO_2$ phases, anatase and rutile. The mean oxide particle size, calculated from the width of the peaks following the Scherrer method, are 25.3 nm and 39.7 nm for anatase and rutile, respectively, as expected for $TiO_2$ P25.

From a number of images like the one shown in Fig. 1, the gold nanoparticle size distribution was established after the measurement of 251 particles (shown as inset). Note that the diameter of the metal particles falls in this catalyst in the 1 nm–6 nm range. The average particle size and gold dispersion that can be estimated from this distribution amount to 3.2 ± 1.1 nm and 36% respectively.

The structural changes taking place after the incorporation of $CeO_2$ can be appreciated in the HAADF-STEM image shown in Fig. 2, which corresponds to the as prepared $CeO_2$(5.4%)/Au(1.5%)/$TiO_2$ sample. Note that in addition to the Au nanoparticles, bright, plate like, contrasts of intermediate intensities are now also observed on the surface of the $TiO_2$ crystallites. These new features correspond to $CeO_2$ structures ($Z_{Ce}$ = 58). The dimensions of these surface structures are just of a few nanometers (< 2 nm), which reveals that, after the impregnation procedure, ceria is well dispersed on top of the surface of the Au/$TiO_2$ system. Concerning morphology, though most of the supported ceria nanostructures are present as very thin, less than 1 nm thick, nanoplates or nanorafts, a small fraction of rounded, 3D type, $CeO_2$ nanoparticles were also found. The assignment of these new contrasts in the HAADF-STEM images to $CeO_2$ nanostructures was confirmed by direct nano-analysis using XEDS-STEM, as it can be seen in Fig. 3. Thus, Fig. 3(a) shows a HAADF-STEM image in which both small, rounded, Au nanoparticles (arrowed with *b*) and nanoraft-like structures (arrowed with *c*) are present. The XEDS-STEM spectrum recorded by placing a 0.5 nm electron probe in the first position, shown in Fig. 3(b), does indeed show the signals of Au and Ti, whereas the spectrum recorded on the latter location shows only the peaks corresponding to Ce and Ti. A significant part of the ceria crystallites were found in contact with gold nanoparticles.

Once the two types of surface structures could be identified, the Au nanoparticle size distribution could be properly established,

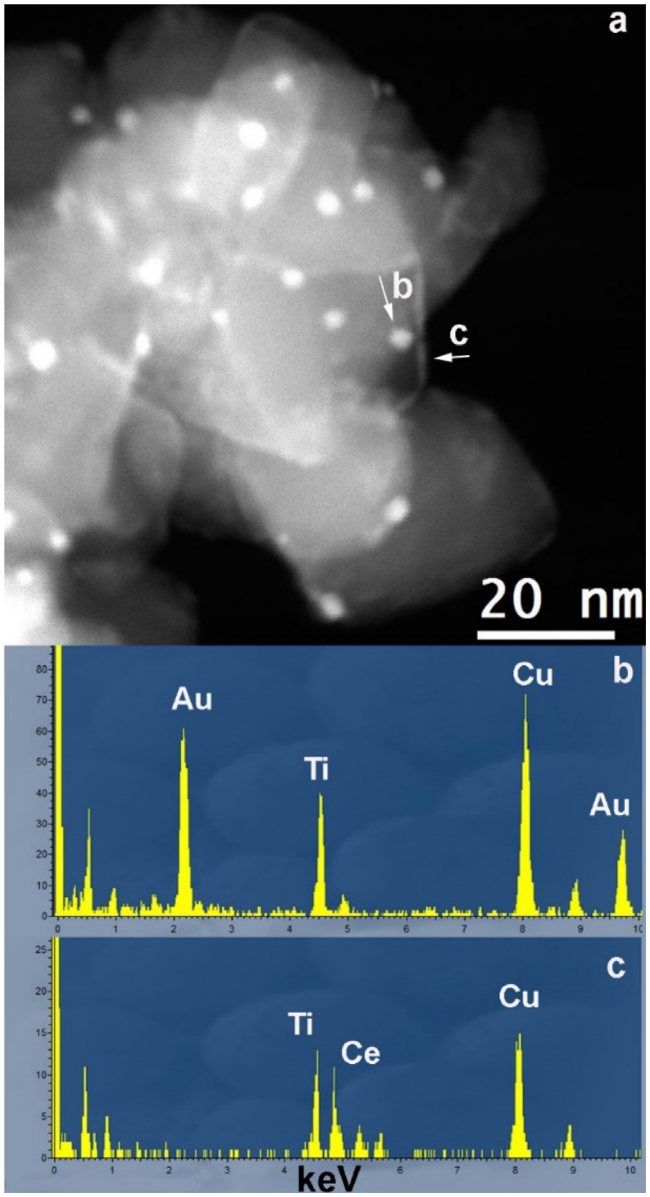


**Fig. 3.** Results of the XEDS-STEM nanoanalytical study performed on the as-prepared $CeO_2$(5.4%)/Au(1.5%)/$TiO_2$ catalyst: (a) HAADF-STEM image; (b) and (c) XEDS spectra recorded on the locations indicated with arrows in (a).

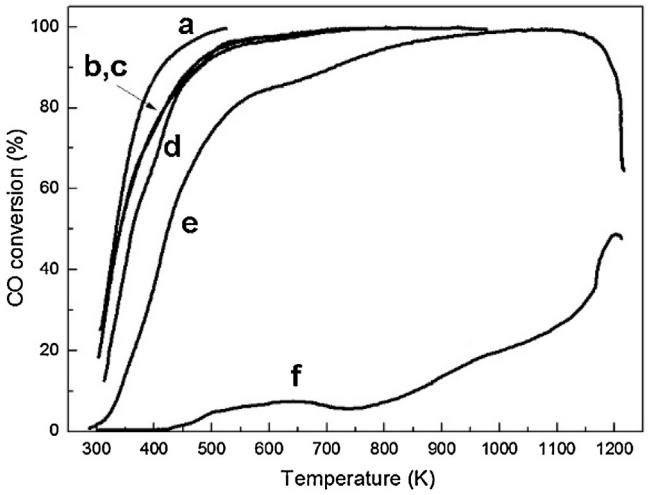


**Fig. 4.** CO oxidation activity tests performed sequentially on the Au(1.5%)/$TiO_2$ WGC catalyst up to 523 K (a), 623 K (b), 773 K (c), 973 K (d), 1223 K (e) and again up to 1223 K (f). After finishing each CO oxidation cycle the sample was cooled down to RT under the reaction mixture.

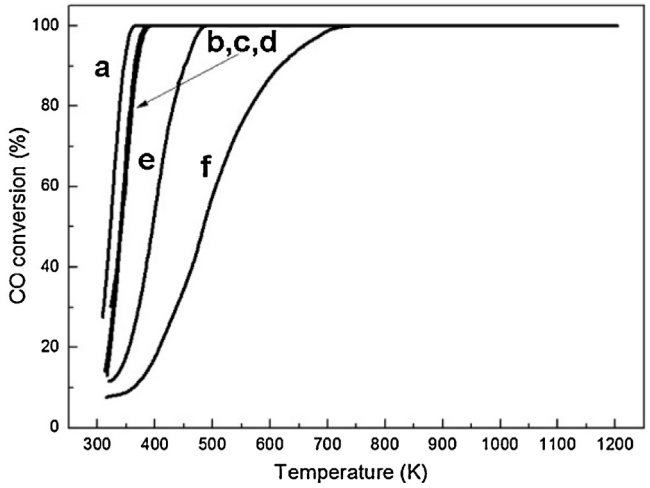


**Fig. 5.** CO oxidation activity tests performed sequentially on the $CeO_2$(5.4%)/Au(1.5%)/$TiO_2$ catalyst up to 523 K (a), 623 K (b), 773 K (c), 973 K (d), 1223 K (e) and again up to 1223 K (f). After finishing each CO oxidation cycle the sample was cooled down to RT under the reaction mixture.

after the analysis of 173 particles, shown as inset in Figure (2). The average metal particle size and metal dispersion in the ceria supported sample were $3.1 \pm 1.5$ nm and 37%, values quite close to those of the starting Au(1.5%)/$TiO_2$ WGC catalyst. Therefore, the addition of $CeO_2$ by incipient wetness impregnation and further oxidation treatment do not lead to significant changes of the gold nanoparticle size distribution. This result is very significant, since it allows a clear comparison of the catalytic performance of the two catalysts. In other words, differences in the catalytic performance between these two materials must be linked to factors other than metal dispersion. This is in fact a quite interesting approach, which can only be reached by a post-modification route as the one used here.

It is important to mention that the addition of ceria doesnít modify the nature or phase distribution of the support. Powder X-ray diffraction shows the presence of peaks corresponding to anatase and rutile, with a mean particle size of 22.7 nm and 38.9 nm, respectively. Values very similar to those corresponding to the reference sample before the addition of ceria. Wider peaks which can be assigned to the $CeO_2$ phase can also be detected, corresponding to a mean particle size of 7.5 nm, in good agreement with STEM data.

### 3.2. Catalytic activity in CO oxidation

The samples were investigated for their catalytic activity towards the oxidation of CO. Previously to the test, an oxidizing pre-treatment at 523 K for 1 h in $O_2$(5%)/He was performed on both catalysts. Figs. 4 and 5 show the results corresponding to the Au(1.5%)/$TiO_2$ WGC and $CeO_2$(5.4%)/Au(1.5%)/$TiO_2$ catalysts respectively.

The first catalytic test was carried out following the CO conversion while the temperature was increased (heating rate 10 K $min^{-1}$) from room temperature up to 523 K, plots marked with (a) in both Figures. A significant improvement of the activity of the Au/$TiO_2$ catalyst is observed after the addition of ceria. Thus, the 50% conversion of CO to $CO_2$ is achieved at 334 K ($T_{50}$) for the Au(1.5%)/$TiO_2$ reference sample, but this temperature decreases to 323 K for

the $CeO_2$ (5.4%)/Au(1.5%)/$TiO_2$ system. More important, the temperature for 100% CO conversion ($T_{100}$) decreases from 508 K to 362 K. So the full conversion of CO is achieved by the ceria modified catalyst at a temperature more than 140 K below that of the Au(1.5%)/$TiO_2$ WGC reference. This improvement in the catalytic activity of the system clearly evidences a promoting effect of $CeO_2$, which correlates with the excellent properties of Au/$CeO_2$ catalysts towards the oxidation of CO. Rodriguez et al. [7] have attributed the improvement in the activity in the WGS reaction over inversed type catalysts consisting of ceria and titania nanoparticles grown on Au(111) thin films to cooperative interactions taking place at the perimeter of the nanoparticles. On its hand, Campbell et al. [36] have pointed out the possible role of electronic interactions in the behavior of $CeO_2$/Au/$TiO_2$. Likewise an enhancement of the oxygen storage capacity of $CeO_2$ in the form of a surface phase [37–39] could also contribute in case that a redox mechanism would prevail in this type of catalysts.

Since stability remains as a critical issue in the performance of supported gold catalysts under high temperature reaction conditions, the modification of the performance of the two catalysts was evaluated in consecutive heating-cooling cycles under the CO:$O_2$ reaction mixture at increasing values of the final temperature, as described in the experimental section. Plots (b) to (f) in Figs. 4 and 5 show the results of the stability tests for the reference and ceria-modified catalysts respectively. The $T_{50}$ and $T_{100}$ values determined from the curves gathered in these plots are summarized in Table 1. According to data in this table, the ceria-modified catalyst prepared in this work shows a much better performance than Au(1.5%)/$TiO_2$ WGC.

In fact, Au(1.5%)/$TiO_2$ WGC catalyst suffers a significant deactivation already after the first reaction cycle at 523 K. Note at this respect that, after reaching this temperature under the reaction mixture during the first catalytic essay, cooling down to RT and starting a second activity test, plot (b) in Fig. 4, the full conversion of CO to $CO_2$ is not achieved within the RT–623 K temperature range. The deactivation effects of this catalyst are also noticeable after the cycles at 623 K and 773 K, plots (c) and (d) in the same Figure, and becomes more severe after the cycle at 923 K, curve (e). In particular, after the cycle at 623 K the $T_{50}$ value does not change with respect to that observed after the previous cycle at 523 K but there is an increase of 228 K in the $T_{100}$ temperature with respect to that of the starting, just preoxidized, catalyst. Likewise, after the cycle at 773 K there is an increase of 28 K and 270 K in the $T_{50}$ and $T_{100}$ values, which points out to a larger deactivation. After the cycle at 973 K there is a clear intensification of the deactivation process of the WGC catalysts, which now show $T_{50}$ and $T_{100}$ values deviating by as much as 91 K and 547 K with respect to the starting catalyst. Finally, after the cycle at the highest temperature, 1223 K, the deactivation of the catalyst is almost complete, as it can be appreciated from plot (f) in Fig. 4. In this latter case, the shape of the ignition curve loses the usual sigmoid-like shape and the catalyst does only reach CO conversion values slightly above 50% at the highest reaction temperature. The $T_{50}$ value in the last catalytic essay increases by 869 K, up to 1203 K.

In contrast to that previously described for the Au(1.5%)/$TiO_2$ WGC catalyst, the behavior of the $CeO_2$(5.4%)/Au(1.5%)/$TiO_2$ sample is much more stable. Deactivation is only very slight after the first cycles at 523 K, 623 K and 773 K, plots (b), (c) and (d) in Fig. 5. The shifts in the $T_{50}$ and $T_{100}$ values are almost the same in these three cases and amount only to 18 K and 21 K. This means that even after the cycle at the highest of these three temperatures, 773 K, the activity of the catalyst remains quite close to that of the just-preoxidized catalyst. It is also very significant that after the cycle at 973 K, plot (e) in Fig. 5, 100% CO conversion is achieved at 485 K, i.e. only 123 K above the value of the untreated catalyst. This value is 570 K below that corresponding to the WGC catalyst, whose $T_{100}$ temperature exceeds one thousand degrees ($T_{100}$ = 1055 K).

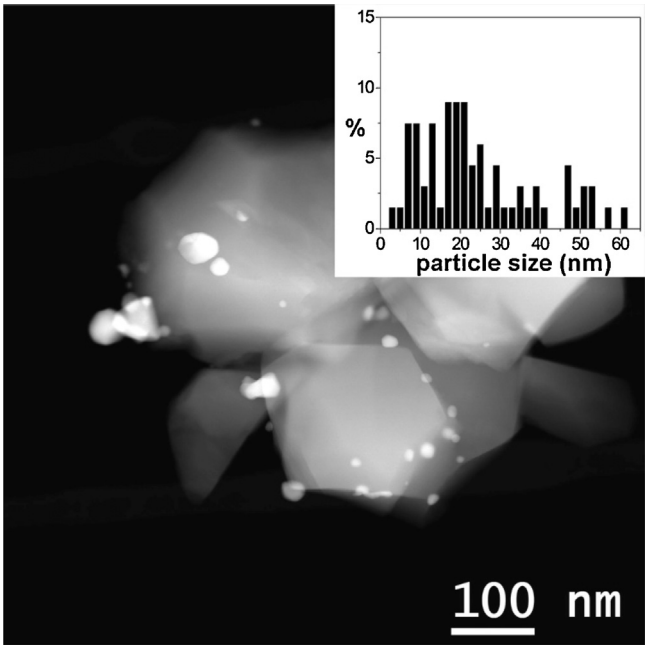


**Fig. 6.** HAADF-STEM image representative of the structure of the Au(1.5%)/$TiO_2$ WGC catalyst after exiting the last CO oxidation cycle performed at the highest temperature, 1223 K. The gold particle size distribution of this catalyst is shown as inset.

Finally, the most remarkable result from this series of catalytic activity measurements is that observed in the CO Conversion-Temperature curve of the ceria-modified catalyst after the cycle at 1223 K, plot (f) in Fig. 5. Note that this ignition curve still maintains the usual sigmoid-like shape and depicts $T_{50}$ and $T_{100}$ values of just 482 K and 735 K, respectively. In the conventional Au(1.5%)/$TiO_2$ catalyst, a very large increase in the $T_{50}$ value is observed between the last two cycles, $\Delta T_{50}$ = 869 K, which clearly evidences a severe deactivation. This change in $T_{50}$ is much smaller, by one order of magnitude, in the case of the $CeO_2$(5.4%)/Au(1.5%)/$TiO_2$ catalyst, $\Delta T_{50}$ = 86 K.

In summary, the results commented above prove a significant improvement in the deactivation behavior of the Au(1.5%)/$TiO_2$ WGC catalyst by deposition of a nanostructured ceria layer using the procedure described in this work.

### 3.3. *Characterization of catalysts after the reaction cycles*

In order to understand the differences between the two catalysts, in terms of changes in their nanostructures during the catalytic essays, both of them were investigated by HAADF-STEM after the last reaction cycle. Thus, Fig. 6 shows a HAADF-STEM image representative of the structure of the Au(1.5%)/$TiO_2$ WGC catalyst after the last reaction test. Note the presence in this case of very large Au nanoparticles (brightest areas in the image). These particles are mostly found on locations of the $TiO_2$ crystallites corresponding to edges, corners or grain boundaries. The analysis of a number of images like that shown in Fig. 6 indicates that the average size of titanium oxide support crystallites has increased dramatically. Peaks attributable to anatase cannot be detected in the Powder X-ray diffraction diagram of this sample, this confirming the total transformation of this phase to rutile, after the catalytic cycles. The average particle size for the final rutile phase is now 37.8 nm. However, the STEM data demonstrates that the oxide particle distribution is very wide and oxide particles larger

**Table 1**
Catalytic oxidation cycles. Temperatures for 50% conversion ($T_{50}$) and 100% conversion ($T_{100}$) for the corresponding samples.

| Catalyst | Pretreatment | Max. Temperature of the Catalytic essay (K) | $T_{50}$ (K) | $T_{100}$ (K) |
|---|---|---|---|---|
| $CeO_2$ (5.4%)/Au(1.5%)/$TiO_2$ | Preox–523 K | 523 | 323 | 362 |
| | CO + $O_2$–523 K | 623 | 341 | 383 |
| | CO + $O_2$–623 K | 773 | 341 | 383 |
| | CO + $O_2$–773 K | 973 | 341 | 384 |
| | CO + $O_2$–973 K | 1223 | 396 | 485 |
| | CO + $O_2$–1223 K | 1223 | 482 | 735 |
| Au(1.5%)/$TiO_2$ | Preox–523 K | 523 | 334 | 508 |
| | CO + $O_2$–523 K | 623 | 341 | [a] |
| | CO + $O_2$–623 K | 773 | 341 | 736 |
| | CO + $O_2$–773 K | 973 | 362 | 778 |
| | CO + $O_2$–973 K | 1223 | 425 | 1055 |
| | CO + $O_2$–1223 K | 1223 | 1203 | [a] |

[a] In these cases 100% conversion was not reached.

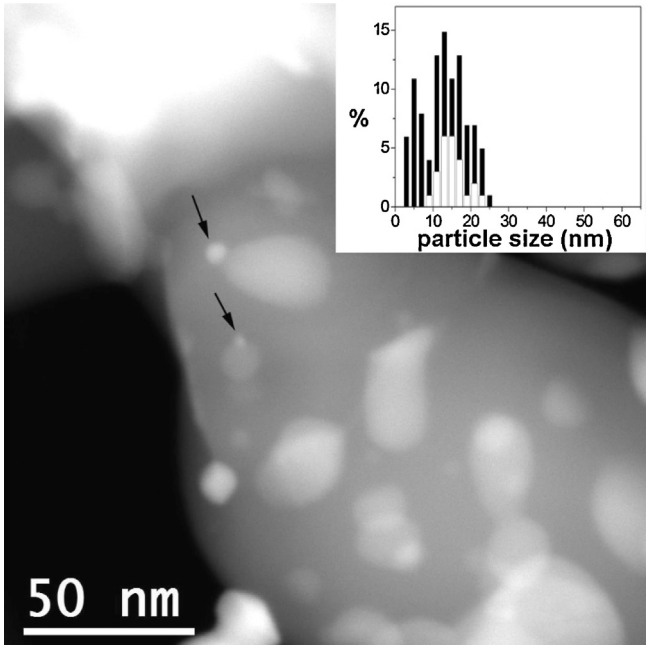


**Fig. 7.** HAADF-STEM image representative of the structure of the $CeO_2$(5.4%)/Au(1.5%)/$TiO_2$ catalyst after exiting the last CO oxidation cycle performed at the highest temperature, 1223 K. The gold particle size distribution of this catalyst is shown as inset.

than 200 nm in size can in fact be found. In parallel with this support grain growth process, gold nanoparticles also undergo a severe process of sintering, as it can be appreciated from the particle size distribution determined from the analysis of more than 100 particles recorded in the HAADF-STEM images (shown as inset in Fig. 6). Now the average Au particle size is 24.0 ± 14.6 nm. The particle size range becomes very wide, reaching particle diameters as large as 60 nm, with only a minor fraction of the distribution below 5 nm (< 10%). These results point out, as expected, to a very poor stability of the gold nanoparticles under reaction conditions involving high temperatures, as it has been the case of the CO oxidation tests performed in this work. This dramatic sintering of the metallic phase must largely contribute to the deactivation effect described above. Sintering of the $TiO_2$ support involves a decrease in the available surface area, which, in turn, brings the supported gold nanoparticles closer together. This would facilitate the occurrence of gold nanoparticle sintering whatever its mechanism could be. Therefore, support crystal growth cannot be disregarded as a factor that facilitates Au nanoparticle sintering.

The nanostructure of the ceria modified catalyst is neatly different, Fig. 7. HAADF-STEM images of this $CeO_2$(5.4%)/Au(1.5%)/$TiO_2$ catalyst evidence still the presence of a large number of very small Au nanoparticles, like those pointed by arrows in Fig. 7. The medium intensity, patch-like, areas observed in these images correspond to the $CeO_2$ nanolayers, which can be quite easily recognized and extend over a few tens of nanometers. Note also, very importantly, how most of the Au nanoparticles are contacting these nanolayers.

To confirm the contrast assignment commented above, XEDS-STEM nanoanalytical studies were performed in spot mode, using an electron probe of roughly 0.5 nm diameter. The results are gathered in Fig. S1 of Supporting information. Note that the XEDS spectra recorded on locations labeled as 1 and 2, which are just the two particles arrowed in the HAADF-STEM image of Fig. 7, do only show, in addition to the signals due to $TiO_2$ and the Cu-grid support, the peaks characteristic of Au. This evidences that they are small Au nanoparticles. Moreover, it also indicates that the Au nanoparticles are not covered on their surfaces by patches of ceria, since in this case both peaks of Ce and Au would have been observed at these locations.

On its hand, the spectra recorded on locations 3 and 4 in Fig. S1, which are just the medium intensity areas in the HAADF-STEM in contact with these nanoparticles, do only depict signals due to Ce, which confirm that these areas correspond to ceria nanolayers. It is therefore feasible to discriminate, on the basis of image contrasts, between the two types of nanostructures present in this aged catalyst; Au nanoparticles and $CeO_2$ nanolayers.

Once the possibility of reliably identifying the two types of particles from their HAADF contrasts was clearly established, a quantitative analysis of all the images recorded on this sample was performed, which provided also quite interesting data. First, as shown in the inset of Fig. 7, the particle size distribution, obtained after the analysis of more than 60 particles, is much narrower than that of the conventional Au(1.5%)/$TiO_2$ catalyst, the largest particles being roughly of 25 nm in diameter. The average particle size in this sample is 12.1 ± 5.8 nm and the corresponding metal dispersion of 9%. During the analysis of the particle size diameters, those Au nanoparticles in contact with the ceria nanolayers were identified, as were also those that remained isolated, apparently not in contact with the $CeO_2$ nanostructures. In the particle size distribution shown as inset in Fig. 7 the contribution of both types of particles is indicated. The former type, those in contact with ceria, are represented by the black bars in the histograms, whereas the white bars correspond to the fraction of isolated Au nanoparticles. As an example, the fraction of Au nanoparticles with diameters between 10 and 12 nm represent 13% of the total number of particles; 3% of them corresponds to Au nanoparticles which are not in contact with ceria (white part of the bar) and 10% to those which are contacting the ceria nanolayers (black part of the bar). Taking this detail into account, the total fraction of Au particles in contact simultaneously with ceria surface layers and the titania support was estimated to amount up to 75%, whereas only 25% are in con-

tact just with the titania crystallites. The average size of the Au nanoparticles in contact with ceria is 12 nm whereas those which are out of contact are slightly larger, 15 nm. More important from a catalytic point of view, the particles with size below 6 nm are in all cases in contact with the ceria nanolayers and represent roughly 25% of the total number of gold particles in the catalyst tested at the highest temperature, 1223 K.

The assignment made above was further corroborated by a more in-depth nanoanalytical study performed on the $CeO_2$(5.4%)/Au(1.5%)/$TiO_2$ catalyst after the aging cycle at 1223 K, using an Aberration Corrected STEM microscope equipped with a very high efficiency XEDS system comprising up to four detectors (ChemiSTEM from FEI) and a high brightness FEG electron source (XFEG). The size of the electron probe in this case was below the angstrom scale, this allowing the detection of the different elements in the catalyst with a very high spatial resolution. The high efficiency of the detection system in conjunction with the high intensity of the electron beam allowed us detecting elements present even in very small nanostructures. Representative element distribution maps and XEDS spectra recorded on this catalyst are gathered in Fig. 8 and S2. In these maps Ti is shown in blue, Ce in green and Au in red color. Note the presence in Fig. 8(a) of a very small Au particle (< 3 nm) (white arrow) stuck to a 10 nm ceria raft (see also the presence of the Au peaks in the spectrum at location 1 and of Ce in location 2 in Fig. S2). In Fig. 8(b) another two Au particles (arrowed in white) are identified by their XEDS signal. The smaller one, on the left side of the map, is clearly contacting a $CeO_2$ raft. In the case of the larger Au particle (close to 20 nm in diameter) observed on the right part of the map, there is also an overlap with a small green area just inside the particle. It is difficult to say in this case, given the projection conditions, if the particle is contacting or not a ceria structure. In any case this second particle is also in the neighborhood of a $CeO_2$ raft. It is therefore clear from the results of this more detailed analytical study that there is a contact between the Au nanoparticles and the ceria rafts deposited on the surface of $TiO_2$.

The analysis of the Powder X-ray diffraction data shows that the textural evolution of the $TiO_2$ support is very similar in both samples, with and without ceria. Thus, the X-ray diffraction diagram of the $CeO_2$/Au/$TiO_2$ system after the catalytic cycles, displays only peaks of the rutile phase and the calculated mean particle size for the $TiO_2$ particles is around 36.0 nm. This behavior is very similar to that of the Au/$TiO_2$ sample after the catalytic cycles. Moreover, the comparison of the X-ray diffraction data from $CeO_2$/Au/$TiO_2$ samples, before and after the cycles, shows a significant sintering of the ceria phase up to an average size of 25.1 nm, in agreement with the STEM studies.

All the results presented above point out that the interaction between the supported ceria rafts and gold nanoparticles must have contributed to limit in an effective way the advancement of the gold sintering process. This limitation of the metal phase sintering could clearly be a major contribution to the enhanced stability of the gold nanoparticles at high temperature and under the reactive environment of the CO oxidation cycles. It is also important to stress that the growth of the particles not in direct contact with the ceria nanolayers is also more limited than in the conventional Au(1.5%)/$TiO_2$ catalyst. In fact these particles range in size from 8 up to 22 nm in the $CeO_2$(5.4%)/Au(1.5%)/$TiO_2$ catalyst after the last catalytic cycle, but they are still much more smaller than those observed in the Au(1.5%)/$TiO_2$ catalyst after the same cycle. For the latter, a significant fraction of particles lye in the 25 nm–60 nm particle size range. The barrier effect played by the ceria nanolayers anchored on the support surface, which could limit migration of both Au atoms and entire Au nanoparticles over the surface of the $TiO_2$ crystallites, plus the special interaction itself between the gold nanoparticles and the ceria surface nanolayers could explain the stabilization effect of the gold nanoparticles [40].

It is also worth noting that the total fraction of more active particles, i.e. those smaller than 5 nm, decreases in the $CeO_2$(5.4%)/Au(1.5%)/$TiO_2$ catalyst after the last catalytic cycle but it still remains in a reasonable value, around 17%. In the conventional Au(1.5%)/$TiO_2$ catalyst after the same catalytic cycle the corresponding value is below 2%. These differences must very likely contribute to both the partial deactivation observed in the $CeO_2$(5.4%)/Au(1.5%)/$TiO_2$ catalyst and the large difference at this respect observed with the conventional, unmodified, WGC catalyst.

### 3.4. Surface nanostructured ceria versus bulk ceria

Apart from the role of the surface ceria nanostructures as activity stabilization component in supported gold titania catalysts evidenced by the whole series of data presented above, it is also worth comparing the catalytic performance of the $CeO_2$(5.4%)/Au(1.5%)/$TiO_2$ catalyst prepared in this work with that of Au dispersed over bulk ceria-zirconia mixed oxides. In the former ceria is present, in very low loadings, as a highly dispersed surface nano-structured component in close contact with gold nanoparticles. In Au/($CeO_2$-$ZrO_2$) catalysts, ceria is present in the form of a bulk oxide, in molar ratios largely exceeding 5%, contacting the gold nanoparticles dispersed on its surface.

Fig. 9 provides catalytic activity data that allow a comparison of these two types of systems. In particular the ignition (conversion vs temperature) curves for CO oxidation for three different catalysts are included: Au(2.6%)/$Ce_{0.62}Zr_{0.38}O_2$ (black line), $CeO_2$(5.4%)/Au(1.5%)/$TiO_2$ as prepared in this work (grey line) and, finally, Au(1.5%)/$TiO_2$ WGC (dashed line). All the catalysts were tested under the same experimental conditions.

From these results it is clear, as already mentioned, that the addition of the ceria nanolayers on top of the titania surface plays a major promoting effect on the activity of the gold nanoparticles present in the Au(1.5%)/$TiO_2$ WGC catalyst. More importantly, note that the activity of the two ceria-containing catalysts is very similar; the $T_{50}$ value is less than 10 K higher for the $CeO_2$(5.4%)/Au(1.5%)/$TiO_2$ catalyst and $T_{100}$ is even smaller in this catalyst than in that based on the bulk ceria-zirconia oxide [2]. If we take into account the gold loadings and metal dispersion values in both catalysts (1.5% and 36% in the case of $CeO_2$(5.4%)/Au(1.5%)/$TiO_2$; 2.6% and 47% in Au(2.6%)/$Ce_{0.62}Zr_{0.38}O_2$ [2]) the catalytic activity data shown in Fig. 9 suggest that the intrinsic activity of the gold atoms exposed at the surface of the catalyst in which ceria is present as a surface phase is much higher than that in which ceria takes part of a bulk mixed oxide.

This is a very significant result, clearly favoring the use of ceria in the form of surface nanostructures instead of incorporating it into bulk-type oxide supports. In other words, it is possible to obtain a catalyst that performs much better, at least in the case of the CO oxidation reaction, using much smaller (one order of magnitude) amounts of cerium (5.4 at% vs 57 at%). Significant improvements are observed both in the intrinsic activity of the gold atoms and, more importantly, in their stability under high temperature reaction conditions. The latter was the major concern of this work.

## 4. Conclusions

The whole set of structural and functional characterization data presented here proves first that it is possible to modify titania supported gold catalysts by the addition of very small amounts of ceria by incipient wetness impregnation and further calcination at low temperatures, without essentially modifying the features of the starting Au nanoparticle system.

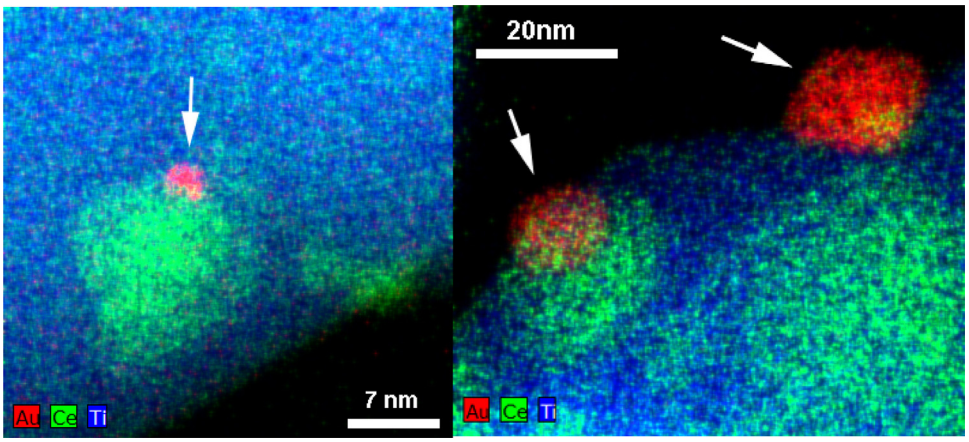


**Fig. 8.** Representative elemental map distributions recorded on the $CeO_2$(5.4%)/Au(1.5%)/$TiO_2$ catalyst after the last CO oxidation cycle performed at 1223 K. Au is shown in red, Ce in green and Ti in blue colors: (left) a region depicting a very small, <3 nm Au particle; (right) another crystallite showing a small and a large Au particle.

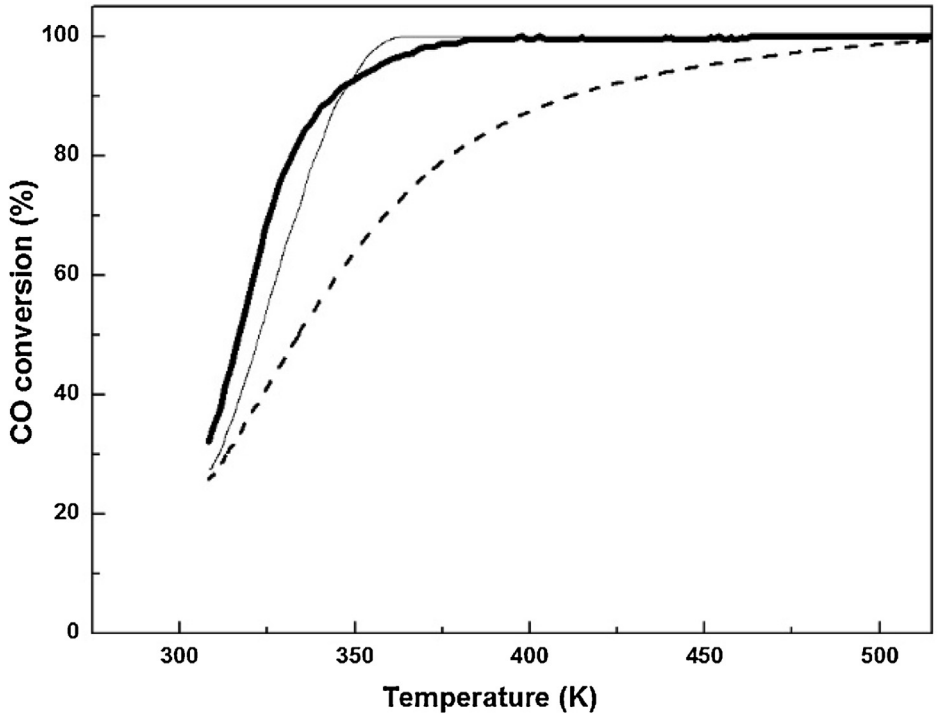


**Fig. 9.** CO oxidation activity tests corresponding to the following catalysts: Au(1.5%)/$TiO_2$ (dashed line), $CeO_2$(5.4%)/Au(1.5%)/$TiO_2$ (grey line) and Au(2.5%)/$Ce_{0.62}Zr_{0.38}O_2$ (black line).

In the case of a sub-monolayer coverage, like the one used in this work, ceria incorporates to the surface mostly in the form of nanometer-sized, sub-nanometer thick, ceria rafts, highly dispersed over the surface of titania crystallites. These ceria nanorafts get in contact with a large fraction of the Au nanoparticles already present on the surface of the titania support without covering their surface. These contacts enable synergistic interactions between the three components of the catalyst (gold, ceria and titania), which result in large improvements of different aspects of the catalytic performance in CO oxidation.

Firstly, there is a promoter effect of ceria onto the activity of the starting gold/titania catalyst. This has been nicely proven taking advantage of the fact that the catalyst modification protocol used in this work does not change the characteristics of the gold particle size distribution of the starting catalyst.

Secondly, and the most remarkable aspect, an improvement in the resistance of the Au nanoparticle system against sintering under CO oxidation conditions cycling between low and very high temperatures (as high as 1223 K) takes place. This extra-stability feature of the catalyst prepared in this work opens a door to applications involving harsh reaction conditions as those established during the operation of TWCs.

Finally, the post-modification route essayed in this work allows preparing catalysts which are more active than others which incorporate Cerium in bulk oxide phases and which use not only higher amounts of this critical element but also of a noble element as it is the case of gold. In this sense, the catalyst here prepared perfectly aligns with new European and North-American directives encouraging the development of alternative materials in which the use of these elements is optimized [31–33].

## Acknowledgements

This work has received financial support from Junta de Andalucía (Project P10-FQM-6766, FQM334 and FQM110), MINECO/FEDER (Projects MAT2013-40823-R, CSD2009-00013, UNCA-10-1E-855). STEM studies were performed at the DME Facilities of SCCYT of University of Cádiz. Financial resources from the European Union Seventh Framework Program under Grant Agreement number 312483-ESTEEM2 (Integrated Infrastructure Initiative) are also acknowledged. M. Tinoco thanks the FPU grants program from the Spanish Ministry of Education.

## Appendix A. Supplementary data

Supplementary data associated with this article can be found, in the online version, at http://dx.doi.org/10.1016/j.apcatb.2016.04.037.

## References

[1] S. Carrettin, P. Concepción, A. Corma, J.M. López Nieto, V.F. Puntes, Nanocrystalline CeO2 increases the activity of Au for CO oxidation by two orders of magnitude, Angew. Chem. Int. Ed. Engl. 43 (2004) 2538–2540, http://dx.doi.org/10.1002/anie.200353570.
[2] E. del Río, G. Blanco, S. Collins, M.L. Haro, X. Chen, J.J. Delgado, et al., CO oxidation activity of a Au/Ceria-Zirconia catalyst prepared by Deposition–Precipitation with urea, Top. Catal. 54 (2011) 931–940, http://dx.doi.org/10.1007/s11244-011-9711-0.
[3] T. Uchiyama, H. Yoshida, Y. Kuwauchi, S. Ichikawa, S. Shimada, M. Haruta, et al., Systematic morphology changes of gold nanoparticles supported on CeO2 during CO oxidation, Angew. Chem. Int. Ed. Engl. 50 (2011) 10157–10160, http://dx.doi.org/10.1002/anie.201102487.
[4] H.Y. Kim, H.M. Lee, G. Henkelman, CO oxidation mechanism on CeO(2)-supported Au nanoparticles, J. Am. Chem. Soc. 134 (2012) 1560–1570, http://dx.doi.org/10.1021/ja207510v.
[5] O. Pozdnyakova, D. Teschner, A. Wootsch, J. Krohnert, B. Steinhauer, H. Sauer, et al., Preferential CO oxidation in hydrogen (PROX) on ceria-supported catalysts, part I: Oxidation state and surface species on Pt/CeO2 under reaction conditions, J. Catal. 237 (2006) 1–16, http://dx.doi.org/10.1016/j.jcat.2005.10.014.
[6] Q. Fu, H. Saltsburg, M. Flytzani-Stephanopoulos, Active nonmetallic Au and Pt species on ceria-based water-gas shift catalysts, Science 301 (2003) 935–938, http://dx.doi.org/10.1126/science.1085721.
[7] J.A. Rodriguez, S. Ma, P. Liu, J. Hrbek, J. Evans, M. Pérez, Activity of CeOx and TiOx nanoparticles grown on Au(111) in the water-gas shift reaction, Science 318 (2007) 1757–1760, http://dx.doi.org/10.1126/science.1150038.
[8] G.J. Hutchings, Catalysis by gold, Catal. Today 100 (2005) 55–61, http://dx.doi.org/10.1016/j.cattod.2004.12.016.
[9] S.J. Freakley, Q. He, C.J. Kiely, G.J. Hutchings, Gold catalysis a reflection on where we are now, Catal. Lett. 145 (2014) 71–79, http://dx.doi.org/10.1007/s10562-014-1432-0.
[10] N. Yi, M. Flytzani-Stephanopoulos, Gold/Ceria, in: Catal. by Mater. with Well-Defined Struct, Elsevier, 2015, pp. 133–158, http://dx.doi.org/10.1016/B978-0-12-801217-8.00005-0.
[11] S. Tsubota, D.A.H. Cunningham, Y. Bando, M. Haruta, Preparation of catalysis VI—scientific bases for the preparation of heterogeneous catalysts, in: Proceedings of the Sixth International Symposium, Elsevier, 1995, http://dx.doi.org/10.1016/S0167-2991(06)81759-3.
[12] E. del Río, D. Gaona, J.C. Hernández-Garrido, J.J. Calvino, M.G. Basallote, M.J. Fernández-Trujillo, et al., Speciation-controlled incipient wetness impregnation: a rational synthetic approach to prepare sub-nanosized and highly active ceria–zirconia supported gold catalysts, J. Catal. 318 (2014) 119–127, http://dx.doi.org/10.1016/j.jcat.2014.07.001.
[13] M. Valden, Onset of catalytic activity of gold clusters on titania with the appearance of nonmetallic properties, Science 281 (1998) 1647–1650, http://dx.doi.org/10.1126/science.281.5383.1647 (80-.).
[14] M. Haruta, When gold is not noble: catalysis by nanoparticles, Chem. Rec. 3 (2003) 75–87, http://dx.doi.org/10.1002/tcr.10053.
[15] M. López-Haro, J.J. Delgado, J.M. Cies, E. Del Rio, S. Bernal, R. Burch, et al., Bridging the gap between CO adsorption studies on gold model surfaces and supported nanoparticles, Angew. Chemie Int. Ed. 49 (2010) 1981–1985, http://dx.doi.org/10.1002/anie.200903403.
[16] Z. Ma, S. Dai, Development of novel supported gold catalysts: a materials perspective, Nano Res. 4 (2010) 3–32, http://dx.doi.org/10.1007/s12274-010-0025-5.
[17] M. Kipnis, Gold in CO oxidation and PROX: The role of reaction exothermicity and nanometer-scale particle size, Appl. Catal. B Environ. 152–153 (2014) 38–45, http://dx.doi.org/10.1016/j.apcatb.2014.01.030.
[18] Y. Guan, W. Song, E.J.M. Hensen, Catalysis by Materials with Well-Defined Structures, Elsevier, 2015, http://dx.doi.org/10.1016/B978-0-12-801217-8.00004-9.
[19] M. López-Haro, J.M. Cíes, S. Trasobares, J. a. Pérez-Omil, J.J. Delgado, S. Bernal, et al., Imaging nanostructural modifications induced by electronic metal-support interaction effects at Au||cerium-based oxide nanointerfaces, ACS Nano 6 (2012) 6812–6820.
[20] X.Y. Liu, A. Wang, T. Zhang, C.-Y. Mou, Catalysis by gold: new insights into the support effect, Nano Today 8 (2013) 403–416, http://dx.doi.org/10.1016/j.nantod.2013.07.005.
[21] M. Tinoco, S. Fernandez-Garcia, M. Lopez-Haro, A.B. Hungria, X. Chen, G. Blanco, et al., Critical influence of nanofaceting on the preparation and performance of supported gold catalysts, ACS Catal. 5 (2015) 3504–3513, http://dx.doi.org/10.1021/acscatal.5b00086.
[22] J.A. Hernández, S.A. Gómez, T.A. Zepeda, J.C. Fierro-González, G.A. Fuentes, Insight into the deactivation of Au/CeO 2Catalysts studied by In situ spectroscopy during the CO-PROX reaction, ACS Catal. 5 (2015) 4003–4012, http://dx.doi.org/10.1021/acscatal.5b00739.
[23] Y. Miyake, S. Tsuji, No Title, EP 1043059 A1, 2000.
[24] P.M. Arnal, M. Comotti, F. Schüth, High-temperature-stable catalysts by hollow sphere encapsulation, Angew. Chem. Int. Ed. Engl. 45 (2006) 8224–8227, http://dx.doi.org/10.1002/anie.200603507.
[25] Z. Ma, S.H. Overbury, S. Dai, Au/MxOy/TiO2 catalysts for CO oxidation: promotional effect of main-group, transition, and rare-earth metal oxide additives, J. Mol. Catal. A Chem. 273 (2007) 186–197, http://dx.doi.org/10.1016/j.molcata.2007.04.007.
[26] K. Zhao, B. Qiao, J. Wang, Y. Zhang, T. Zhang, A highly active and sintering-resistant Au/FeOx-hydroxyapatite catalyst for CO oxidation, Chem. Commun. (Camb). 47 (2011) 1779–1781, http://dx.doi.org/10.1039/c0cc04171h.
[27] J. Wang, A.-H. Lu, M. Li, W. Zhang, Y.-S. Chen, D.-X. Tian, et al., Thin porous alumina sheets as supports for stabilizing gold nanoparticles, ACS Nano 7 (2013) 4902–4910, http://dx.doi.org/10.1021/nn401446p.
[28] C. Chen, M. Shi, M. Cargnello, P. Fornasiero, C.B. Murray, R.J. Gorte, Au@TiO2Core–Shell nanostructures with high thermal stability, Catal. Lett. 144 (2014) 1939–1945, http://dx.doi.org/10.1007/s10562-014-1351-0.
[29] B. Puértolas, Á. Mayoral, R. Arenal, B. Solsona, A. Moragues, S. Murcia-Mascaros, et al., High-Temperature stable gold nanoparticle catalysts for application under severe conditions: the role of TiO 2 nanodomains in structure and activity, ACS Catal. 5 (2015) 1078–1086, http://dx.doi.org/10.1021/cs501741u.
[30] H. Zhu, Z. Ma, S.H. Overbury, S. Dai, Rational design of gold catalysts with enhanced thermal stability: post modification of Au/TiO2 by amorphous SiO2 decoration, Catal. Lett. 116 (2007) 128–135, http://dx.doi.org/10.1007/s10562-007-9144-3.
[31] European Commission, Critical Raw Materials for the EU, Report of the Ad-hoc Working Group on Defining Critical Raw Materials, 2010, http://dx.doi.org/10.1002/eji.200839120, IL-17-Producing.
[32] U.S. department of energy, Critical materials strategy, 2010.
[33] E.A. Chu, S., Critical Materials Strategy, DOE/PI-0009, 2011.
[34] Gold reference catalysts, Gold Bull. 36, 24-24, 2003 10.1007/BF03214864.
[35] B. Ohtani, O.O. Prieto-Mahaney, D. Li, R. Abe, What is Degussa (Evonik) P25? Crystalline composition analysis, reconstruction from isolated pure particles and photocatalytic activity test, J. Photochem. Photobiol. A Chem. 216 (2010) 179–182, http://dx.doi.org/10.1016/j.jphotochem.2010.07.024.
[36] C.T. Campbell, Catalyst-support interactions: electronic perturbations, Nat. Chem. 4 (2012) 597–598, http://dx.doi.org/10.1038/nchem.1412.
[37] M.P. Yeste, J.C. Hernández-Garrido, D.C. Arias, G. Blanco, J.M. Rodríguez-Izquierdo, J.M. Pintado, et al., Rational design of nanostructured, noble metal free, ceria-zirconia catalysts with outstanding low temperature oxygen storage capacity, J. Mater. Chem. A 1 (10) (2013) 4836, http://dx.doi.org/10.1039/c3ta00016h.
[38] G. Zhou, J. Hanson, R.J. Gorte, A thermodynamic investigation of the redox properties of ceria–titania mixed oxides, Appl. Catal. A Gen. 335 (2008) 153–158, http://dx.doi.org/10.1016/j.apcata.2007.11.011.
[39] J.B. Park, J. Graciani, J. Evans, D. Stacchiola, S.D. Senanayake, L. Barrio, et al., Gold, copper, and platinum nanoparticles dispersed on CeO(x)/TiO(2)(110) surfaces: high water-gas shift activity and the nature of the mixed-metal oxide at the nanometer level, J. Am. Chem. Soc. 132 (2010) 356–363, http://dx.doi.org/10.1021/ja9087677.
[40] A. Zaleska, Doped-TiO2: a review, Recent Pat. Eng. 2 (2008) 157–164, http://dx.doi.org/10.2174/187221208786306289.